MENP: an open-source MATLAB implementation of multipole expansion for nanophotonics

Hinamoto, Tatsuki

Fujii, Minoru

(Citation)
OSA Continuum,4(5):1640-1648

(Issue Date)
2021-05-15

(Resource Type)
journal article

(Version)
Version of Record

(URL)
https://hdl.handle.net/20.500.14094/90009626

Research Article Vol. 4, No. 5 / 15 May 2021 / OSA Continuum 1640

MENP: an open-source MATLAB implementation of multipole expansion for nanophotonics

TATSUKI HINAMOTO[1,2] AND MINORU FUJII[1,3]

[1]Department of Electrical and Electronic Engineering, Graduate School of Engineering, Kobe University, Kobe 657-8501, Japan
[2]tatsuki.hinamoto@gmail.com
[3]fujii@eedept.kobe-u.ac.jp

Abstract: In modern nanophotonics, multipolar interference plays an indispensable role to realize novel optical devices represented by metasurfaces with unprecedented functionalities. Not only to engineer sub-wavelength structures that constitute such devices but also to realize and interpret unnatural phenomena in nanophotonics, a program that efficiently carries out multipole expansion is highly demanded. MENP is a MATLAB program for computation of multipole contributions to light scattering from current density distributions induced in nanophotonic resonators. The main purpose of MENP is to carry out post-processing of a rigid multipole expansion for full-field simulations that in principle provide the information of all near- and far-field interactions (*e.g.*, as a total scattering cross section). MENP decomposes total scattering cross sections into partial ones due to electric and magnetic dipolar and quadrupolar terms based on recently developed exact multipole expansion formulas. We validate the program by comparing results for ideal and realistic nanospheres with those obtained with the Mie theory. We also demonstrate the potential of MENP for analysis of anapole states by calculating the multipole expansion under the long-wavelength approximation, which enables us to introduce toroidal dipole moments.

1. Introduction

The emergence of all-dielectric nanophotonics as an alternative to plasmonics has opened up a door toward the engineering of scattering behaviors by sub-wavelength nanophotonic resonators with an unprecedented degree of freedom. [1–5] The operation of all-dielectric nanophotonics relies on Mie resonances accompanied by light confinement within sub-wavelength nanostructures made of high-refractive-index materials. One of the important features of the Mie resonance in stark contrast to plasmonics is the possession of electric and magnetic dipole and higher-order multipole resonances. [6–9] It has been proposed and demonstrated that engineering of these modes can remarkably improve the performance of optical components including metasurfaces with the help of the low-loss nature of all-dielectric Mie resonators. [10] The development of all-dielectric nanophotonics could impact a wide range of fields, including optical elements [11], detectors [12,13], light-sources [14,15], sensing [16], nanophotonic inks [17], and so on.

It has been demonstrated that multipolar interference between a series of resonant modes leads to fascinating phenomena. [10] For example, Huygens sources, individual scatterers which radiate light only into forward direction, can be realized with non-magnetic structures by the far-field interference between electric and magnetic dipole scatterings. [18–22] Such zero-backward-scattering occurs at the condition where the electric (p) and magnetic (m) dipole moments have the same scattering amplitudes with in-phase (so-called the first Kerker condition: $p - m/c = 0$, where c is the speed of light.). [21] The concept of the Kerker-type directionality has been extended into almost zero-forward scattering (the anti-Kerker condition: $p + m/c = 0$) and transverse scattering. [23] Another intriguing phenomenon is an anapole state which exhibits no radiating field; the phenomenon is interpreted as a result of destructive interference

#425189 https://doi.org/10.1364/OSAC.425189
Journal © 2021 Received 17 Mar 2021; revised 29 Apr 2021; accepted 30 Apr 2021; published 11 May 2021

OSA CONTINUUM

between electric and toroidal dipole moments. [24] Note that several different interpretations are possible for the anapole state. [25–28] The radiationless state is of importance in realizing invisible photodetectors with minimum cross-talk between the other elements and to confine electromagnetic energy inside subwavelength resonators. [28–33]

Because most of the fascinating phenomena in nanophotonics, including the above mentioned Kerker condition and non-radiating anapole state, stem from multipolar interferences of scattered fields between multiple optical resonances, an analysis based on multipole expansion is essential for understanding and engineering optical properties of nanophotonic resonators. [34–36] Although analytical electromagnetic calculation such as the Mie theory [37] naturally includes the multipole analysis, no analytical expressions of optical responses are available for most structures except for some simple ones such as a sphere. For the computation of electromagnetic responses of complex structures, full-field simulation techniques based on finite-difference time-domain (FDTD) method, finite-element method (FEM), boundary element method (BEM), discrete-dipole approximation (DDA), and so on are thus utilized. In commercially available simulation software, it is straightforward to obtain electric and magnetic field distributions and some typical quantities such as *total* scattering and absorption cross sections. However, decomposition of the total scattering into multipole contributions can be problematic because such analysis is not often provided in public, requiring us more or less effort for coding of complex expressions. To this end, a program that efficiently computes multipole expansion from the electric field distributions is highly demanded.

In addition to the well-known formulation of multipole expansion found in textbooks of electrodynamics, [38] some expressions have been developed for easier implementation in designing optical resonators. [27,34–36] The formulations can be classified into several methods depending on the basis (Spherical or Cartesian) and the approaches (scattered fields or induced currents), and those based on induced current density distributions in the Cartesian coordinate system is often adopted in nanophotonics applications. Up to now, an exact expression recently derived by Alaee and coauthors is, in our opinion, one of the most straightforward formulations. [35] Besides, the expression derived under the long-wavelength approximation is also commonly utilized with the introduction of *so-called* toroidal moments which are higher-order terms of electric moments. [27,39]

Inspired by the work by Alaee, *et al*. and substantial demands in the field, here we develop an open-source MATLAB code that computes multipole expansion for nanophotonics (MENP). MENP provides an efficient computation using matrix processing in MATLAB to treat four-dimensional (4D) matrices of electric field distributions. This work consists of the following sections. After summarizing the theoretical expressions implemented in MENP, we explain the overview of the program. We then validate our implementation by computing the exact multipole expansion for a lossless nanosphere with a combination of FDTD and MENP, followed by a comparison to analytically obtained results. The procedure is also carried out for a silicon nanosphere with complex refractive indices. Finally, we apply MENP to a silicon nanodisk to show the existence of the anapole state based on the multipole expansion under the long-wavelength approximation. Although the MENP has the best compatibility with FDTD solutions (Lumerical Inc.) because of the authors' simulation environment, it is a versatile program and is not limited to the combination with FDTD. MENP will significantly contribute to nanophotonics fields by providing physical insights into multipolar interferences in various structures.

2. Theory

First, we describe the exact expression of multipole expansion reported in [35]. As a starting point, let us define a problem: a resonator in free space is illuminated by a plane wave with an electric field amplitude $|\boldsymbol{E}_{\mathbf{inc}}| = E_0$ at the frequency f. The basis is a Cartesian coordinate system, and a position vector can be defined as $\boldsymbol{r} = (x, y, z)$. When incident light excites the resonator, the

OSA CONTINUUM

induced current density distributions $\boldsymbol{J}(\boldsymbol{r})$ can be obtained from the electric field distributions $\boldsymbol{E}(\boldsymbol{r})$ by

$$\boldsymbol{J}(\boldsymbol{r}) = -i\omega\varepsilon_0(n^2-1)\boldsymbol{E}(\boldsymbol{r}) \tag{1}$$

, where ω is the angular frequency, ε_0 is the permittivity of free space, and n is the refractive indices of the resonator. Note that $\boldsymbol{J}(\boldsymbol{r})$ corresponds to displacement current distributions in the case of dielectric Mie resonators. The multipole moments, that is, electric dipole ($\boldsymbol{p}$), magnetic dipole ($\boldsymbol{m}$), electric quadrupole ($\hat{Q}^{\mathrm{e}}$), magnetic quadrupole ($\hat{Q}^{\mathrm{m}}$), can be derived as [35]:

$$\begin{aligned}
p_\alpha &= -\tfrac{1}{i\omega}\left[\int J_\alpha j_0(kr)\mathrm{d}^3\boldsymbol{r} + \tfrac{k^2}{2}\int\{3(\boldsymbol{r}\cdot\boldsymbol{J})r_\alpha - r^2J_\alpha\}\tfrac{j_2(kr)}{(kr)^2}\mathrm{d}^3\boldsymbol{r}\right]\\
m_\alpha &= \tfrac{3}{2}\int(\boldsymbol{r}\times\boldsymbol{J})_\alpha\tfrac{j_1(kr)}{kr}\mathrm{d}^3\boldsymbol{r}\\
\hat{Q}^{\mathrm{e}}_{\alpha\beta} &= -\tfrac{3}{i\omega}\left[\int\{3(r_\beta J_\alpha + r_\alpha J_\beta) - 2(\boldsymbol{r}\cdot\boldsymbol{J})\delta_{\alpha\beta}\}\tfrac{j_1(kr)}{kr}\mathrm{d}^3\boldsymbol{r}\right.\\
&\quad +2k^2\int\{5r_\alpha r_\beta(\boldsymbol{r}\cdot\boldsymbol{J}) - r^2(r_\alpha J_\beta + r_\beta J_\alpha)\\
&\quad \left.-r^2(\boldsymbol{r}\cdot\boldsymbol{J})\delta_{\alpha\beta}\}\tfrac{j_3(kr)}{(kr)^3}\mathrm{d}^3\boldsymbol{r}\right]\\
\hat{Q}^{\mathrm{m}}_{\alpha\beta} &= 15\int\{r_\alpha(\boldsymbol{r}\times\boldsymbol{J})_\beta + r_\beta(\boldsymbol{r}\times\boldsymbol{J})_\alpha\}\tfrac{j_2(kr)}{(kr)^2}\mathrm{d}^3\boldsymbol{r},
\end{aligned} \tag{2}$$

where $\alpha,\beta = x,y,z$ and k is the wavenumber. Note that $j_n(\rho)$ denotes the spherical Bessel function defined by $j_n(\rho) = \sqrt{\pi/2\rho}\ J_{n+1/2}(\rho)$, where $J_n(\rho)$ is the Bessel function of first kind.

Using the above derived multipole moments, we can now calculate a total scattering cross section by [38]

$$C^{\mathrm{total}}_{\mathrm{sca}} = \frac{k^4}{6\pi\varepsilon_0^2|E_0|}\left[\sum\left(|\boldsymbol{p}|^2 + \left|\frac{\boldsymbol{m}}{c}\right|^2\right) + \frac{1}{120}\sum\left(|\hat{Q}^{\mathrm{e}}|^2 + \left|\frac{k\hat{Q}^{\mathrm{m}}}{c}\right|^2\right) + \ldots\right]. \tag{3}$$

As can be seen, the total scattering cross section is a simple sum of partial scattering cross sections from different multipoles (*i.e.*, $C^{\boldsymbol{p}}_{\mathrm{sca}}, C^{\boldsymbol{m}}_{sca}, C^{\hat{Q}^e}_{\mathrm{sca}}, C^{\hat{Q}^m}_{\mathrm{sca}}$).

Next, we show the expression under the long-wavelength approximation. It is known that the approximated expression can be derived by making an approximation to the spherical Bessel functions. [27,35,39]. The multipole moments are expressed as:

$$\begin{aligned}
p_\alpha &\approx -\tfrac{1}{i\omega}\left[\int J_\alpha\mathrm{d}^3\boldsymbol{r} + \tfrac{k^2}{10}\int\{(\boldsymbol{r}\cdot\boldsymbol{J})r_\alpha - 2r^2J_\alpha\}\mathrm{d}^3\boldsymbol{r}\right]\\
m_\alpha &\approx \tfrac{1}{2}\int(\boldsymbol{r}\times\boldsymbol{J})_\alpha\mathrm{d}^3\boldsymbol{r}\\
\hat{Q}^{\mathrm{e}}_{\alpha\beta} &\approx -\tfrac{1}{i\omega}\left[\int\{3(r_\beta J_\alpha + r_\alpha J_\beta) - 2(\boldsymbol{r}\cdot\boldsymbol{J})\delta_{\alpha\beta}\}\mathrm{d}^3\boldsymbol{r}\right.\\
&\quad +\tfrac{k^2}{14}\int\{4r_\alpha r_\beta(\boldsymbol{r}\cdot\boldsymbol{J}) - 5r^2(r_\alpha J_\beta + r_\beta J_\alpha)\\
&\quad \left.+2r^2(\boldsymbol{r}\cdot\boldsymbol{J})\delta_{\alpha\beta}\}\mathrm{d}^3\boldsymbol{r}\right]\\
\hat{Q}^{\mathrm{m}}_{\alpha\beta} &\approx \int\{r_\alpha(\boldsymbol{r}\times\boldsymbol{J})_\beta + r_\beta(\boldsymbol{r}\times\boldsymbol{J})_\alpha\}\mathrm{d}^3\boldsymbol{r}.
\end{aligned} \tag{4}$$

The total scattering cross sections can be obtained in the same expression as Eq. (3).

Finally, we introduce toroidal moments to the multipole family. Because the higher-order term of the electric dipole moment can be regarded as the toroidal dipole moment ($\boldsymbol{T}$), the expression can be rewritten as

$$\begin{aligned}
p_\alpha &\approx -\tfrac{1}{i\omega}\int J_\alpha\mathrm{d}^3\boldsymbol{r}\\
T_\alpha &\approx \tfrac{1}{10c}\int\{(\boldsymbol{r}\cdot\boldsymbol{J})r_\alpha - 2r^2J_\alpha\}\mathrm{d}^3\boldsymbol{r}.
\end{aligned} \tag{5}$$

OSA CONTINUUM

The corresponding total scattering cross section is:

$$C_{\mathrm{sca}}^{\mathrm{total}} = \frac{k^4}{6\pi\varepsilon_0^2|E_0|}\left[\sum\left(|\boldsymbol{p}+ik\boldsymbol{T}|^2+\left|\frac{\boldsymbol{m}}{c}\right|^2\right)+\frac{1}{120}\sum\left(|\hat{Q}^{\mathrm{e}}|^2+\left|\frac{k\hat{Q}^{\mathrm{m}}}{c}\right|^2\right)+\ldots\right]. \tag{6}$$

Note that here we introduced only toroidal dipole, and a higher-order toroidal moment is included in the electric quadrupole moment. It is also possible to treat the higher-order terms of the electric quadrupole moment as a *so-called* toroidal quadrupole moment. From Eq. (6), the anapole condition can be derived as $\boldsymbol{p} + ik\boldsymbol{T} = 0$.

3. Benchmark

3.1. Overview

In Fig. 1, we show the overview describing the calculation flow of MENP (see Code 1 [40]) to obtain scattering spectra decomposed into multipoles. First, the electric field distributions in a resonator or resonators are simulated in an arbitrary program (Fig. 1(a)). Typically, the simulation is carried out for a plane wave excitation with an amplitude of 1 V/m in air (*i.e.,* with a background refractive index of 1). The electric fields around the resonator should be recorded at each point in a discretized simulation mesh in three-dimension (3D; x, y, z) in the frequency domain (f), leading three (E_x, E_y, E_z) 4D matrices of the field distributions ($\boldsymbol{E}(x, y, z, f)$). To obtain induced current distributions within the resonator, it is convenient to extract refractive index distributions at the same mesh ($n(x, y, z, f)$) because the data outside the resonator vanishes when $n = 1$ (see Eq. (1)). To pass the data together with arrays of coordinates (x, y, z, f) to MENP, they are saved all-in-one MATLAB .mat file named as `ENxyzf.mat`. For convenience, we provide a Lumerical script `EField2MAT.lsf`, which exports the needed data from a project file (.fsp) of FDTD Solutions, in `/lumerical_script` directory.

Once the electric field distributions are obtained, MENP carries out the post-processing of multipole expansion. It is worth noting that MENP is designed for not loop-based but *vectorized* calculations of the 4D matrices, providing a better appearance of the code and faster computing in MATLAB. As shown in Fig. 1(b), MENP is constituted of two MATLAB functions. One is `E2J.m`, which converts the electric field distributions to current density distributions based on Eq. (1). The other (one of the following functions) calculates multipole moments (either exact or approximated ones) and partial and total scattering cross sections:

- `exactME.m`: Exact multipole expansion using Eq. (2).
- `approxME.m`: Multipole expansion under the long-wavelength approximation using Eq. (4).
- `toroidalME.m`: Multipole expansion under the long-wavelength approximation with toroidal dipole moment using Eq. (5).

They return scattering cross sections as a function of frequency.

3.2. Usage

The practical usage of MENP can be understood by looking into demo files:
`/demo_sphere/demo_exact.m` (based on exact expressions; Eq. (2))
`/demo_sphere/demo_approx.m` (based on approximated expressions; Eq. (4))
`/demo_disk/demo_toroidal.m` (based on approximated expressions with toroidal dipole; Eq. (5)).

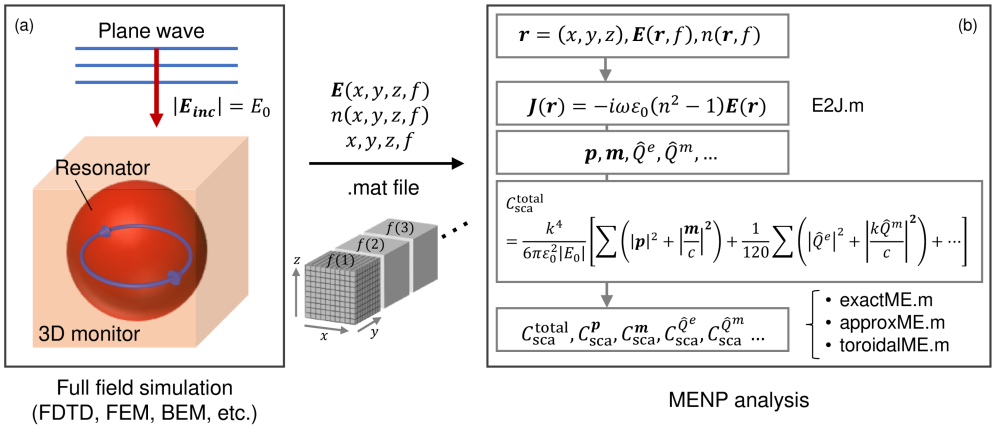

Fig. 1. Overview of the calculation flow with MENP. (a) Calculation of electric fields ($\boldsymbol{E}(x,y,z,f)$) within a nanophotonic resonator under the illumination of a plane wave ($\boldsymbol{E_{inc}}$) with an amplitude E_0. This step is typically done using full-field simulation techniques such as FDTD, FEM, BEM, etc. (b) MENP reads the electric field distributions passed from the simulator. Note that the data should be packaged into .mat file format together with refractive index ($n(x,y,z,f)$) and one-dimensional arrays of axes (x,y,z,f). After the conversion of the electric field distributions into current density ones by `E2J.m` MENP computes multipole moments (electric dipole: $\boldsymbol{p}$, magnetic dipole: $\boldsymbol{m}$, electric quadrupole: $\hat{Q}^e$, magnetic quadrupole: $\hat{Q}^m$), followed by calculations of scattering cross sections.

The installation of the MENP can be done by simply adding a path of `/MENP` directory to the MATLAB search path:

```
addpath(../MENP);
```

Next, one loads `ENxyzf.mat` in which $\boldsymbol{E}, n, x, y, z, f$ are saved. The loaded variables are then passed to the main function, for example:

```
[Cp,Cm,CQe,CQm,Csum]=exactME(x,y,z,f,Ex,Ey,Ez,n_x,n_y,n_z);
```

The returned variables are partial scattering cross sections and the sum of them (*i.e.*, total scattering cross section up to quadrupoles).

3.3. Demonstration

We validate the MENP implementation by calculating the exact multipole expansion for a lossless dielectric nanosphere and comparing the results to the Mie theory. The electric field distributions were obtained by FDTD Solutions (Lumerical Inc.). The simulation setup is schematically shown in Fig. 2(a). The resonator is a lossless nanosphere with a refractive index of 4. A diameter was set to 180 nm to exhibit dipolar and quadrupolar Mie resonances in the visible spectrum. To capture the electric field distributions, a 3D discrete Fourier transform (DFT) monitor (230 nm×230 nm×230 nm) was utilized together with a 3D index monitor that has the same dimension. As a light source, x-polarized plane wave was injected along the z-axis using a total-field scattered-field (TFSF) source (280 nm×280 nm×280 nm). The simulation domain (1.2 μm×1.2 μm×1.2 μm) were defined by perfectly matched layers in all boundaries. In the domain, Yee cells were automatically defined by a graded mesh, except for a region around the resonator where a 4 nm square mesh was overridden. Additionally, a closed monitor consisting of six DFT monitors were added in the scattered field region to measure total scattering cross sections in simulation. After the simulation, multipole contributions were computed with MENP.

Scattering cross sections obtained with FDTD and MENP (`exactME.m`) are shown in Fig. 2(b) with symbols. For comparison, analytically calculated spectra, the Mie theory, for the same

OSA CONTINUUM

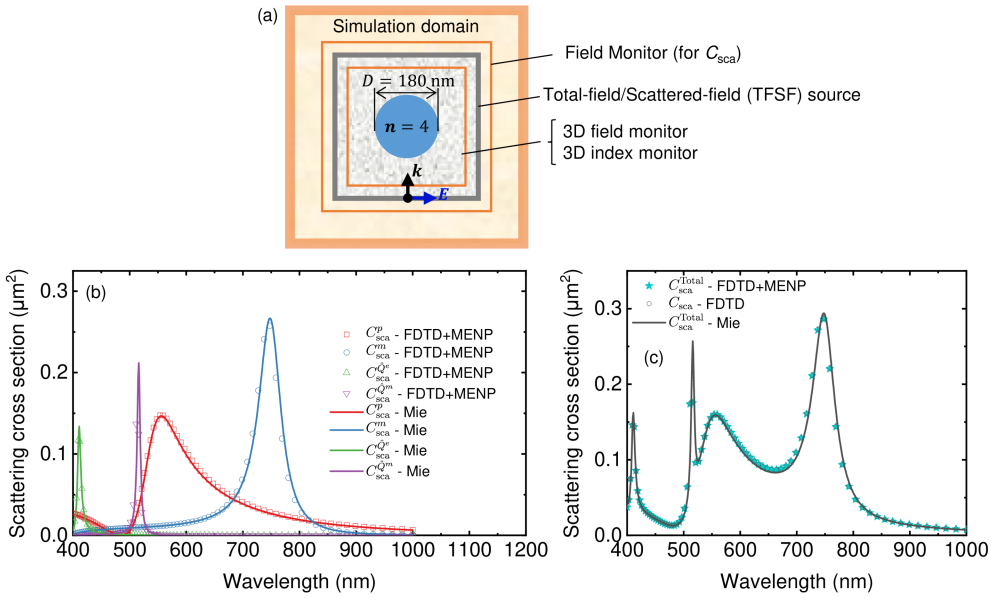

Fig. 2. Benchmark of `exactME.m` for a lossless nanosphere with a refractive index $n = 4$ and a diameter $D = 180$ nm. (a) Schematic illustration of a simulation setup in the full-field simulation. (b,c) Calculated scattering cross sections (b) from each multipole contribution and (c) a total of them (plots with symbols). For comparison, those calculated with a rigid analytical solution, the Mie theory, is shown with solid lines.

configuration are shown with solid lines. One can see quantitative agreement for all the spectra. The nice agreement can be attributed to the exact expression of the multipole expansion beyond the long-wavelength approximation; the approximated computation (`approxME.m`) results in deviation, especially in the short wavelength range (see Fig. S1. in Supplement 1). Note that the accuracy of the entire calculation is determined by that of input datasets. The small deviation in Fig. 2(b), such as a slight blue-shift of the magnetic dipole resonance, is caused by the numerical error not in MENP but in FDTD simulation. Figure 2(c) compares total scattering obtained by three approaches. The plots with stars were calculated by summing up partial scattering cross sections calculated by MENP. Circles were the data obtained directly in FDTD using a monitor surrounding the TFSF source. The solid line is the spectrum obtained from the Mie theory into which up to 10th order resonances are included. Likewise, the spectra show good agreement.

We move on to a benchmark for a resonator made of realistic material. Here, we applied `exactME.m` to a silicon nanosphere with a diameter of 200 nm. The complex refractive indices were adopted from literature by E. Palik. [41] A simulation setup similar to that for Fig. 2 was constructed, but the mesh overriding around the resonator was reduced to 8 nm. The simulated plots (symbols) in Fig. 3 perfectly tracks the analytical spectra (solid lines) as well. One can now see that the higher-order dipole resonances around the wavelength range from 400 to 500 nm are adequately reproduced.

As the implementation has been validated, MENP can now be applied to arbitrary structures. As a demonstration for a specific application in nanophotonics, we demonstrate a multipole analysis on anapole states. The structure here consists of a silicon nanodisk with a diameter and height of 310 and 50 nm, respectively, as shown in Fig. 4(a). As described above, the analysis of the anapole state requires the introduction of a toroidal dipole moment. Accordingly, `toroidalME.m` was applied to the electric field distributions computed in the same manner.

OSA CONTINUUM

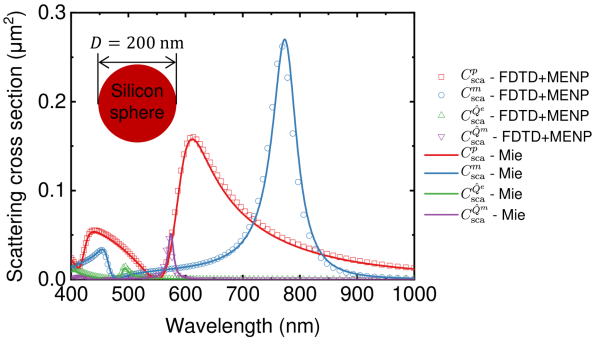

Fig. 3. Benchmark for scattering cross sections of a silicon nanosphere with a complex refractive index [41] and diameter $D = 200$ nm. The multipole contributions computed with FDTD and MEMP and those obtained with the Mie theory are plotted with colored symbols and solid lines, respectively.

The computed partial scattering cross sections are plotted in Fig. 4(b) and are in accordance with those in literature. [24] Different from the result based on exact expressions, the total scattering is not just a summation of multipolar contributions and exceeded by the electric dipolar scattering. This is because the electric and the toroidal dipoles have crosstalk as shown in Eq. (6), which leads to the constructive interference of the radiation. In this way, the dip in total scattering (black band in Fig. 4(b)) occurs when the contributions of electric and toroidal dipoles match (*i.e.*, anapole state). For the anapole condition, the phases of the moments are also important to cancel out the radiation perfectly. The phase of multipole moments can be extracted as a complex argument in computation. Figure 4(c) shows the phases of the electric dipole and toroidal dipole (as $-ik\boldsymbol{T}$). One can see that the lines cross each other around the anapole wavelength, and thus the anapole condition ($\boldsymbol{p} = -ik\boldsymbol{T}$) is satisfied. A supplementary code `toroidalME_phase.m` is also provided in the MENP package. Although we demonstrated the features of MENP for dielectric Mie resonators, it can also be applied to plasmonic materials.

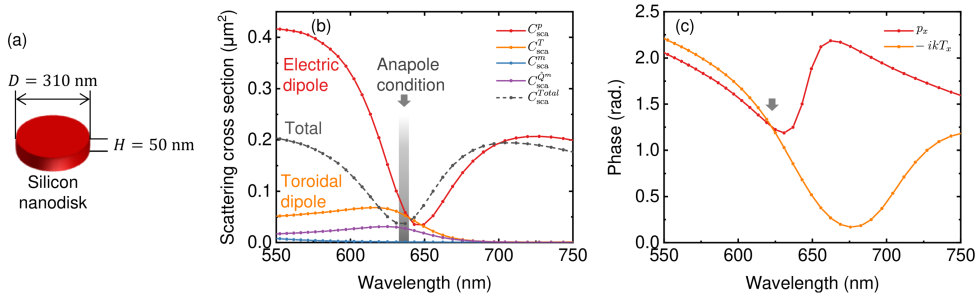

Fig. 4. Multipole analysis for a silicon nanodisk by `toroidalME.m`. (a) Schematic of a simulation model composed of a silicon nanodisk with a diameter of 310 nm and a height of 50 nm. (b) Scattering cross sections of total and multipole contributions obtained by FDTD and MENP. The anapole state, a minimum of the total scattering due to the suppression of electric and toroidal dipolar scatterings, is shown by a dark line. (c) Plots of phases, that is the arguments of complex electric (p_x, red line) and toroidal dipole ($-ikT_x$, orange line) moments. The anapole condition ($\boldsymbol{p} = -ik\boldsymbol{T}$) is satisfied at the wavelength designated by an arrow.

OSA CONTINUUM

Finally, we would like to depict limitation and capability of MENP. First, the program is designed for optical frequencies, implying that magnetic permeabilities of constituting materials must be one ($\mu = 1$). Second, MENP mainly focuses on individual structures, and thus it returns scattering cross sections as an output. It also works for periodic structures for the calculation of multipole moments; however, the returned values (scattering cross sections) are not physically meaningful quantities. In periodic structures, we recommend extracting multipole moments or linking the multipole moments to reflection/transmission coefficients. [42] Third, the accuracy of the results is basically limited by the input datasets since MENP is a post-processing program. By keeping these points in mind, we believe MENP would be a helpful tool for the community.

4. Summary and outlook

In summary, we have presented an open-source MATLAB program MENP designed for efficient computation of multipole expansion in nanophotonics. The program is based on the recently developed exact expression of a multipole expansion and provides the post-analysis for commonly utilized simulation software such as FDTD and FEM. The validity and correctness of the program are demonstrated by comparing the results with analytically obtained quantities. The implementation of multipole expansion under the long-wavelength approximation is also presented to explain the excitation of the anapole state with the help of toroidal dipole moment in a nanodisk. Given the increasing interest in various multipolar interferences in nanophotonics, MENP may have a significant impact on nanophotonics as well as plasmonics community by helping researchers to interpret the physical meaning of scattering-based phenomena.

Funding. Japan Society for the Promotion of Science (18J20276, 18KK0141, 21H01748).

Acknowledgments. T. Hinamoto. acknowledges the support under Grant-in-Aid for JSPS Research Fellows.

Disclosures. The authors declare no conflicts of interest.

Data availability. The data for this work is available as Code 1 (Ref. [40]).

Supplemental document. See Supplement 1 for supporting content.

References

1. Y. Kivshar, "All-dielectric meta-optics and non-linear nanophotonics," Natl. Sci. Rev. **5**(2), 144–158 (2018).
2. S. Jahani and Z. Jacob, "All-dielectric metamaterials," Nat. Nanotechnol. **11**(1), 23–36 (2016).
3. A. I. Kuznetsov, A. E. Miroshnichenko, M. L. Brongersma, Y. S. Kivshar, and B. Luk'yanchuk, "Optically resonant dielectric nanostructures," Science **354**(6314), aag2472 (2016).
4. R. Won, "Into the 'Mie-tronic' era," Nat. Photonics **13**(9), 585–587 (2019).
5. I. Staude, T. Pertsch, and Y. S. Kivshar, "All-Dielectric Resonant Meta-Optics Lightens up," ACS Photonics **6**(4), 802–814 (2019).
6. W. Liu and Y. S. Kivshar, "Multipolar interference effects in nanophotonics," Philos. Trans. R. Soc., A **375**(2090), 20160317 (2017).
7. A. B. Evlyukhin, S. M. Novikov, U. Zywietz, R. L. Eriksen, C. Reinhardt, S. I. Bozhevolnyi, and B. N. Chichkov, "Demonstration of Magnetic Dipole Resonances of Dielectric Nanospheres in the Visible Region," Nano Lett. **12**(7), 3749–3755 (2012).
8. A. I. Kuznetsov, A. E. Miroshnichenko, Y. H. Fu, J. Zhang, and B. Luk'yanchuk, "Magnetic light," Sci. Rep. **2**(1), 492 (2012).
9. T. Hinamoto, S. Hotta, H. Sugimoto, and M. Fujii, "Colloidal Solutions of Silicon Nanospheres toward All-Dielectric Optical Metafluids," Nano Lett. **20**(10), 7737–7743 (2020).
10. S. Kruk and Y. Kivshar, "Functional Meta-Optics and Nanophotonics Governed by Mie Resonances," ACS Photonics **4**(11), 2638–2649 (2017).
11. M. Khorasaninejad, W. T. Chen, R. C. Devlin, J. Oh, A. Y. Zhu, and F. Capasso, "Metalenses at visible wavelengths: Diffraction-limited focusing and subwavelength resolution imaging," Science **352**(6290), 1190–1194 (2016).
12. S. Yi, M. Zhou, Z. Yu, P. Fan, N. Behdad, D. Lin, K. X. Wang, S. Fan, and M. Brongersma, "Subwavelength angle-sensing photodetectors inspired by directional hearing in small animals," Nat. Nanotechnol. **13**(12), 1143–1147 (2018).
13. P. Fan, U. K. Chettiar, L. Cao, F. Afshinmanesh, N. Engheta, and M. L. Brongersma, "An invisible metal-semiconductor photodetector," Nat. Photonics **6**(6), 380–385 (2012).
14. A. F. Cihan, A. G. Curto, S. Raza, P. G. Kik, and M. L. Brongersma, "Silicon Mie resonators for highly directional light emission from monolayer MoS2," Nat. Photonics **12**(5), 284–290 (2018).

OSA CONTINUUM

15. S. T. Ha, Y. H. Fu, N. K. Emani, Z. Pan, R. M. Bakker, R. Paniagua-Domínguez, and A. I. Kuznetsov, "Directional lasing in resonant semiconductor nanoantenna arrays," Nat. Nanotechnol. **13**(11), 1042–1047 (2018).
16. O. Yavas, M. Svedendahl, and R. Quidant, "Unravelling the Role of Electric and Magnetic Dipoles in Biosensing with Si Nanoresonators," ACS Nano **13**(4), 4582–4588 (2019).
17. H. Sugimoto, T. Okazaki, and M. Fujii, "Mie Resonator Color Inks of Monodispersed and Perfectly Spherical Crystalline Silicon Nanoparticles," Adv. Opt. Mater. **8**(12), 2000033 (2020).
18. P. R. Wiecha, A. Cuche, A. Arbouet, C. Girard, G. Colas Des Francs, A. Lecestre, G. Larrieu, F. Fournel, V. Larrey, T. Baron, and V. Paillard, "Strongly Directional Scattering from Dielectric Nanowires," ACS Photonics **4**(8), 2036–2046 (2017).
19. Y. Yang, A. E. Miroshnichenko, S. V. Kostinski, M. Odit, P. Kapitanova, M. Qiu, and Y. S. Kivshar, "Multimode directionality in all-dielectric metasurfaces," Phys. Rev. B **95**(16), 165426 (2017).
20. Y. H. Fu, A. I. Kuznetsov, A. E. Miroshnichenko, Y. F. Yu, and B. Luk'yanchuk, "Directional visible light scattering by silicon nanoparticles," Nat. Commun. **4**(1), 1527 (2013).
21. R. Alaee, R. Filter, D. Lehr, F. Lederer, and C. Rockstuhl, "A generalized Kerker condition for highly directive nanoantennas," Opt. Lett. **40**(11), 2645 (2015).
22. H. Sugimoto, T. Hinamoto, and M. Fujii, "Forward to Backward Scattering Ratio of Dielectric–Metal Heterodimer Suspended in Almost Free-Space," Adv. Opt. Mater. **7**(20), 1900591 (2019).
23. H. K. Shamkhi, K. V. Baryshnikova, A. Sayanskiy, P. Kapitanova, P. D. Terekhov, P. Belov, A. Karabchevsky, A. B. Evlyukhin, Y. Kivshar, and A. S. Shalin, "Transverse scattering and generalized kerker effects in all-dielectric mie-resonant metaoptics," Phys. Rev. Lett. **122**(19), 193905 (2019).
24. A. E. Miroshnichenko, A. B. Evlyukhin, Y. F. Yu, R. M. Bakker, A. Chipouline, A. I. Kuznetsov, B. Luk'yanchuk, B. N. Chichkov, and Y. S. Kivshar, "Nonradiating anapole modes in dielectric nanoparticles," Nat. Commun. **6**(1), 8069 (2015).
25. B. Luk'yanchuk, R. Paniagua-Domínguez, A. I. Kuznetsov, A. E. Miroshnichenko, and Y. S. Kivshar, "Suppression of scattering for small dielectric particles: anapole mode and invisibility," Philos. Trans. R. Soc., A **375**(2090), 20160069 (2017).
26. J. S. Totero Gongora, G. Favraud, and A. Fratalocchi, "Fundamental and high-order anapoles in all-dielectric metamaterials via Fano–Feshbach modes competition," Nanotechnology **28**(10), 104001 (2017).
27. K. V. Baryshnikova, D. A. Smirnova, B. S. Luk'yanchuk, and Y. S. Kivshar, "Optical Anapoles: Concepts and Applications," Adv. Opt. Mater. **7**(14), 1801350 (2019).
28. S.-Q. Li and K. B. Crozier, "Origin of the anapole condition as revealed by a simple expansion beyond the toroidal multipole," Phys. Rev. B **97**(24), 245423 (2018).
29. G. Grinblat, Y. Li, M. P. Nielsen, R. F. Oulton, and S. A. Maier, "Enhanced Third Harmonic Generation in Single Germanium Nanodisks Excited at the Anapole Mode," Nano Lett. **16**(7), 4635–4640 (2016).
30. L. Xu, M. Rahmani, K. Zangeneh Kamali, A. Lamprianidis, L. Ghirardini, J. Sautter, R. Camacho-Morales, H. Chen, M. Parry, I. Staude, G. Zhang, D. Neshev, and A. E. Miroshnichenko, "Boosting third-harmonic generation by a mirror-enhanced anapole resonator," Light: Sci. Appl. **7**(1), 44 (2018).
31. F. Monticone, D. Sounas, A. Krasnok, and A. Alù, "Can a Nonradiating Mode Be Externally Excited? Nonscattering States versus Embedded Eigenstates," ACS Photonics **6**(12), 3108–3114 (2019).
32. L. Wei, Z. Xi, N. Bhattacharya, and H. P. Urbach, "Excitation of the radiationless anapole mode," Optica **3**(8), 799 (2016).
33. J. A. Parker, H. Sugimoto, B. Coe, D. Eggena, M. Fujii, N. F. Scherer, S. K. Gray, and U. Manna, "Excitation of Nonradiating Anapoles in Dielectric Nanospheres," Phys. Rev. Lett. **124**(9), 097402 (2020).
34. R. Alaee, C. Rockstuhl, and I. Fernandez-Corbaton, "Exact Multipolar Decompositions with Applications in Nanophotonics," Adv. Opt. Mater. **7**(1), 1800783 (2019).
35. R. Alaee, C. Rockstuhl, and I. Fernandez-Corbaton, "An electromagnetic multipole expansion beyond the long-wavelength approximation," Opt. Commun. **407**, 17–21 (2018).
36. P. Grahn, A. Shevchenko, and M. Kaivola, "Electromagnetic multipole theory for optical nanomaterials," New J. Phys. **14**(9), 093033 (2012).
37. G. Mie, "Beiträge zur Optik trüber Medien, speziell kolloidaler Metallösungen," Ann. Phys. **330**(3), 377–445 (1908).
38. J. D. Jackson, *Classical Electrodynamics*, 3rd ed. (Wiley, 1998).
39. E. A. Gurvitz, K. S. Ladutenko, P. A. Dergachev, A. B. Evlyukhin, A. E. Miroshnichenko, and A. S. Shalin, "The High-Order Toroidal Moments and Anapole States in All-Dielectric Photonics," Laser Photonics Rev. **13**, 1800266 (2019).
40. T. Hinamoto and M. Fujii, "Multipole Expansion for NanoPhotonics (MENP)," GitHub (2020) [retrieved 3 March 2021], https://github.com/Hinamoooon/MENP.
41. Edward D. Palik, *Handbook of Optical Constants of Solids* (Academic Press, 1998).
42. P. D. Terekhov, V. E. Babicheva, K. V. Baryshnikova, A. S. Shalin, A. Karabchevsky, and A. B. Evlyukhin, "Multipole analysis of dielectric metasurfaces composed of nonspherical nanoparticles and lattice invisibility effect," Phys. Rev. B **99**(4), 045424 (2019).